Microstructural Characteristics and Mechanical Properties of Welded Joints and Base Material of Ultra-Supercritical Pipelines Before and After Service

Haifeng Jiang *

Datang Yuncheng Power Generation Co., Ltd, Heze, Shangdong, China

* Corresponding Author Email: hfeng_jiang@126.com

Abstract. This study investigated the microstructural evolution and mechanical property degradation of ultra-supercritical welded joints and base material (HR3C steel) before and after service. Mechanical property tests, including tensile and impact property tests, were conducted. The results show that the tensile strength, yield strength, elongation, and impact properties of the welded joints and base material after service were lower than those of unserviced specimens. Furthermore, optical microscopy, scanning electron microscopy, and transmission electron microscopy were used to observe the welded joint and base material specimens before and after service. In the initial state, the welded joints and base material had an austenitic microstructure and a diffusely distributed strengthening phase with the composition NbCrN. Moreover, high-temperature exposure led to precipitation processes. After service, Cr-rich M23C6 carbides with a chain-like structure precipitated near the grain boundaries of the welded joints and base material, leading to the aggregation of voids at the grain boundaries. This indicates that the coarsened M23C6 carbides at the grain boundaries negatively affect grain boundary strength, which is the main factor causing the reduction in steel plasticity and toughness. In addition, NbCrN mainly precipitated inside the grains, accompanied by dislocation pinning. The inhibitory effect of the dispersed particles on the dislocations allows the steel to maintain strength properties comparable to the initial state after service. However, the gradual deposition of NbCrN eventually degraded the strength properties.

Keywords: HR3C, long-term service, precipitates, property degradation, microstructural evolution.

1. Background

With the rapid growth of China's economy, the demand for electricity is also rising. Thermal power generation is still the mainstay of China's power supply. However, traditional thermal power units face issues such as outdated technology, low power-generation efficiency, and serious environmental pollution. To address these problems, large-capacity, high-efficiency ultra-supercritical units have become a key research direction for the development and supply of electric power. This is of great significance for the sustainable development of thermal power. As the components operating in the harshest conditions within ultra-supercritical boilers, superheaters and reheaters are subjected to high temperature, high pressure, and corrosion from steam and flue gases for extended periods. As a result, the microstructure and properties of their metallic tube materials will inevitably deteriorate. The deterioration of key devices severely impacts the operational safety of the equipment, shortens its working life, and introduces various hidden hazards, seriously limiting the development of power station units. Therefore, the development of advanced boiler tube materials is imperative. In practice, the ideal material for boiler heated tubes should possess several key properties. First, it should have high endurance strength to ensure long-term stable operation in high-temperature and high-pressure environments; high oxidation resistance; high corrosion resistance; and excellent welding performance to facilitate processing and connection during manufacturing and maintenance. In addition, it should maintain microstructure stability, sufficient ability to absorb impact energy, and low manufacturing costs over long-term service to meet both safety and economic requirements for widespread use in power station boilers. HR3C (25Cr-20Ni-Nb-N) steel is a 25Cr-20Ni type austenitic heat-resistant steel developed by Sumitomo Chemical Co., Ltd., in the 1980s by adding 0.25%~0.6% Nb and 0.15%~0.35% N to 25Cr-20Ni TP310H steel [1]. Owing to solution

strengthening and precipitation strengthening, HR3C heat-resistant steel has good high-temperature creep strength, high-temperature oxidation resistance, and flue gas corrosion resistance [2-3]. It has been applied to the manufacture of superheater and reheater components, with operating temperatures not exceeding 700°C [4-5]. With the gradual increase in the steam parameters of thermal power units, the working environment of typical pipelines in boilers has become increasingly harsh and demanding. The performance of HR3C is limited when operation in high-pressure steam environments of 630~650°C [6-8]. Typical microstructural evolution occurs in austenitic heat-resistant steels during long-term high-temperature creep or aging, causing changes in mechanical properties, which in turn affect the reliability and safety of ultra-supercritical units. The transition zone formed by the differences in the microstructure, composition, and properties of welded joints is the weak link for safe operation under high-temperature conditions and is the source of failures in components such as superheater tubes and reheater tubes in ultra-supercritical units [9-12]. Therefore, it is necessary to explore the microstructural evolution of welded joints and base material after long-term service and their impact on mechanical properties.

HR3C and C-HRA-5 steels have been shown to develop $M_{23}C_6$ carbides, NbCrN phases, Laves phases, σ phases, and Cu-rich particles after high-temperature creep or long-term aging [13]. The precipitation of these phases is responsible for the initial increase in the strength properties of the steel [14]; however, after prolonged high-temperature exposure, changes in the amount and morphology of the precipitated secondary phases can degrade the mechanical properties. A refined mixture of $M_{23}C_6$ carbide and Laves phase precipitates on grain boundaries, both of which grow rapidly owing to their relatively low thermodynamic stability to form a continuous distribution. This reduces the cohesion strength of the grain boundaries, leading to the degradation of the material's mechanical properties. Through interactions with dislocations, Cu-rich particles dispersed inside the grains and the NbCrN phase influence the strength and hardness of the steel during aging. NbCrN, which is more stable than Cu-rich particles, maintains a positive effect on the properties of the steel during longer-term aging [15]. In addition, creep significantly promotes the precipitation of these phases as well as the generation of voids and cracks, accelerating the evolution of the microstructure and the deterioration of the material properties relative to long-term aging. Early research on the welding of dissimilar steels focused on the impact of the welding process on joint performance. In-depth studies on the microstructural evolution of dissimilar steel joints after long-term service and its impact on performance are lacking. Considering that heat-resistant steel undergoes microstructural evolution during long-term service, leading to reduced lifespan, it is of great significance to investigate the microstructural evolution of dissimilar steel welded joints to ensure the safe operation of thermal power units.

Focusing on the mechanical properties and microstructure of welded joints and base material (HR3C steel) of ultra-supercritical pipelines after actual service, this paper investigates the relationship between microstructural evolution and mechanical property degradation by comparing the joints and base material before service with those after 4000 hours of service at 620°C.

2. Materials and Methods

2.1. Test Materials

The welded joints and HR3C steel used in this study were sourced from the field service pipelines of the 660MW primary reheat ultra-supercritical boiler (model HG-1988/29.3-YM5) at Weixian County Power Plant. These pipelines operated at a service temperature of 620°C and had been in service for 4000 hours, with observable cracks on the inner walls. The welded joints were fabricated from HR3C steel and C-HRA-5 steel using gas tungsten arc welding (GTAW). The chemical composition of the base material (HR3C steel) is presented in Table 2-1, while the chemical composition of C-HRA-5 steel is provided in Table 2-2. The specific welding process parameters are detailed in Table 2-3. The welding current, voltage, and speed were 170 A, 11 V, and 9 mm/min, respectively. A ERNiCrCoMo-1 wire, whose composition is shown in Table 2-4, was used.

Table 2-1. Chemical composition of HR3C steel (wt.%)

C	Si	Mn	P	S	Ni	Nb	Cr	N
0.056	0.45	1.13	0.017	0.005	18.91	0.38	24.91	0.24

Table 2-2. Chemical composition of C-HRA-5 steel (wt.%)

C	Si	Mn	P	S	Cu	Cr	Ni	W	Co	Nb	Mo	N
0.07	0.20	0.38	0.019	0.001	3.00	22.20	24.79	3.40	1.56	0.46	0.09	0.21

Table 2-3. Welding process parameters for welded joints

Welding method	Welding current/A	Welding Voltage/V	Welding speed ($mm \cdot s^{-1}$)	Protective gas	Gas flow rate ($L \cdot min^{-1}$)
GTAW	170	11	9	Argon	15-20

Table 2-4. Chemical composition of welding wire (wt.%)

C	Mn	Si	P	S	Mo	Cu
0.10	1.0	1.0	0.03	0.015	10.0	0.50

2.2. Microstructural Characterization

Dissimilar steel welded joints and HR3C steel specimens were cut from the pipelines before and after service for microstructural observation. The metallographic specimens were prepared by grinding and polishing with sandpaper, followed by etching with a solution of 5 g $CuSO_4 \cdot 5H_2O$ + 25 ml HCl + 50 ml H_2O. Microstructural studies were conducted using an Olympus GX51 optical microscope (OM) and Zeiss Sigma 300 scanning electron microscope (SEM) equipped with an energy-dispersive X-ray spectrometer (EDS). Physical characterization was performed using a Tecnai G2 F30 transmission electron microscope (TEM).

2.3. Mechanical Property Tests

Room-temperature tensile tests were conducted on dissimilar steel welded joints and HR3C steel specimens before and after service. The design and machining of the specimens followed the GB/T 228.1-2021 standard "Metallic materials, Tensile testing, Part 1: Method of test at room temperature." Standard tensile specimens with a circular cross-section were sampled longitudinally from the pipeline. Three tensile specimens were taken from both the weld zone and the base material area of the welded joints, and the average value of the measurements was used. Fig.1 shows the location and a schematic of the tensile specimen sampling.

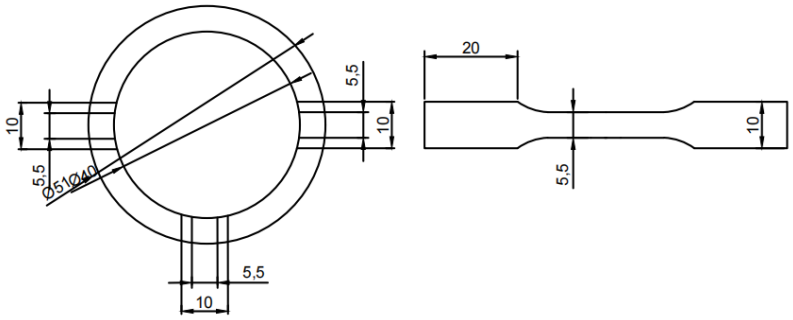

Figure 1. Location and schematic of tensile specimen sampling

Impact tests were performed on dissimilar steel welded joints and HR3C steel before and after service. The specimens were taken along the longitudinal direction of the pipeline. According to the ASTM E23-18 standard, small-size Charpy (simply supported beam) V-notch impact specimens were prepared with dimensions of 55mm×10mm×2.5mm. At least three specimens were subjected to each impact toughness test, and the average of the measurements was used as the final result to minimize

the effects of random errors. Fig.2 shows the location and a schematic of the impact specimen sampling.

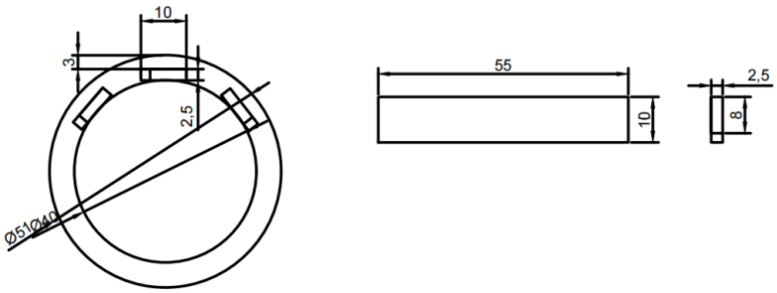

Figure 2. Location and schematic of impact specimen sampling

3. Experimental Results and Discussion

3.1. Analysis of Mechanical Property Test Results

3.1.1. Mechanical Properties and Fracture Morphology of HR3C Steel

Compared with the mechanical properties of the initial specimen, all those of the HR3C steel decreased after service, as shown in Fig.3. For the initial specimen, the yield strength was 380 MPa, the ultimate tensile strength was 790 MPa, the elongation was 51.5%, and the impact toughness was 31 J. After 4000 hours of service at 620°C, the specimen had a yield strength of 740 MPa, an ultimate tensile strength of 360 MPa, an elongation of 36%, and an impact toughness of 22 J.

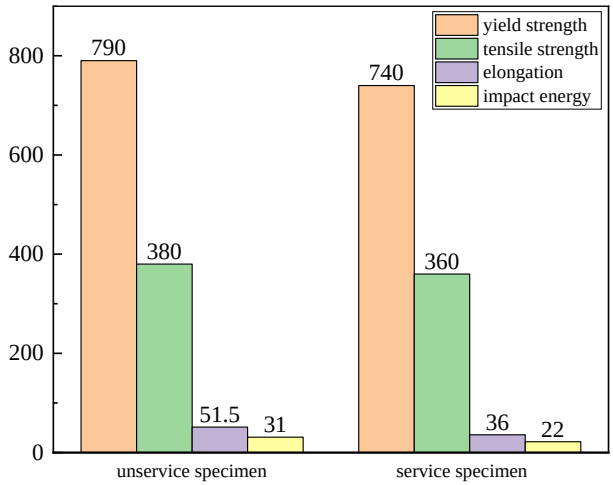

Figure 3. Changes in mechanical properties of HR3C steel before and after service

The tensile fracture morphology of HR3C steel after 4000 hours of service at 620°C is shown in Fig.4(a)–(d). The macroscopic fracture was black and relatively smooth, with obvious icosahedral features, indicating the emergence of intergranular fracture in the HR3C steel after service. The fracture morphology of the Charpy V-notched impact specimens at room temperature is shown in Fig.4(e)–(h). These specimens displayed the same patterns and characteristics as the tensile specimens. The impact and tensile specimens primarily underwent intergranular fracturing, where the fracture morphology was significantly influenced by the precipitation of the secondary phase at the grain boundaries. The greater the amount of secondary phase at the grain boundary, the rougher the grain boundary section and the lower the number of secondary cracks. Under high temperature and stress, the secondary phase, which precipitates and grows at the grain boundaries, strengthens the grain boundaries and hinders grain boundary sliding. Subsequent microstructural analysis revealed that the main precipitates are the $M_{23}C_6$ and NbCrN Z-phases. The $M_{23}C_6$ phase precipitates along the grain boundaries and broadens the grain boundaries as it grows. The lack of Cr between the crystals can easily cause intergranular corrosion, leading to the formation of defects such as voids. In

a long-term high-temperature creep environment, microcracks form, which also affects the mechanical properties. Thus, coarsened carbides on grain boundaries negatively impact grain boundary strength, reduce grain boundary hardness, and cause significant intergranular brittleness, resulting in intergranular brittle fracture and a substantial reduction in impact toughness. The secondary phase diffusely precipitated within the grains is a fine NbCrN Z-phase, which is highly stable at high temperatures and contributes to precipitation strengthening and improved strength.

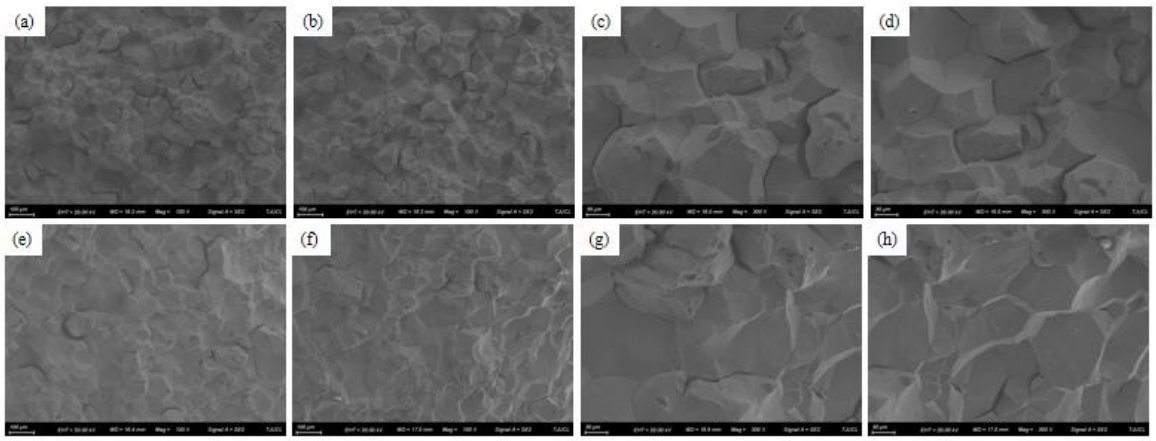

Figure 4. Typical fracture morphology of HR3C steel specimens after service: (a)–(d) Tensile fracture morphology and (e)–(h) impact fracture morphology

3.1.2. Mechanical Properties and Fracture Morphology of Welded Joints

Fig.5 shows the mechanical properties of the welded joints before and after service. It can be seen that the mechanical properties of the specimens decreased after service. For the initial specimen, the yield strength was 455 MPa, the ultimate tensile strength was 745 MPa, the elongation was 54.5%, and the impact toughness was 54 J. After 4000 hours of service at 620°C, the specimen had a yield strength of 693 MPa, an ultimate tensile strength of 379 MPa, an elongation of 21%, and an impact toughness of 13 J.

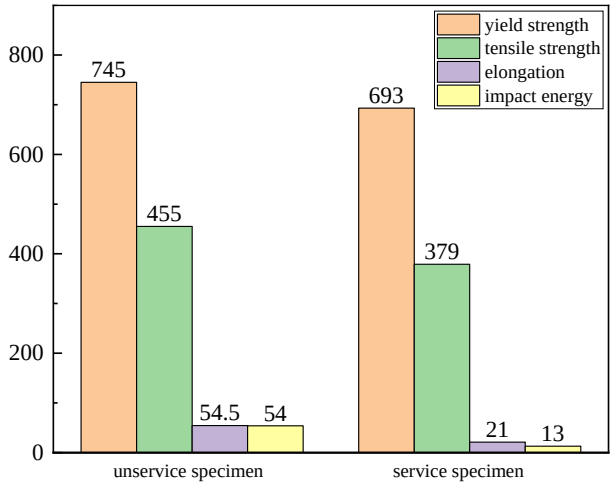

Figure 5. Changes in mechanical properties of welded joints before and after service

The tensile fracture morphology of the welded joints after 4000 hours of service at 620°C is shown in Fig.6(a)–(d). The morphological characteristics were similar to those of the tensile fracture of HR3C steel: the macroscopic fracture was black and smooth, possessed distinct icosahedral features, and displayed no obvious necking phenomenon, indicating that the intergranular fracture in the welded joints emerged after service. The fracture morphology of the Charpy V-notched impact specimens at room temperature is shown in Fig.6(e)–(h). It can be seen that the morphological characteristics differed significantly from those of the impact fracture of HR3C steel. The

macroscopic fracture appeared bright gray and rough, dimples aggregated at the fracture, and small precipitated particles were visible at the base of the dimples. Overall, the fracture also showed cleavage, indicating a mixed mode of transgranular fracture and intergranular fracture. As the strain rate increased, the tendency for brittle fracturing also increased, and the fracture toughness decreased. However, for some materials, an excessive strain rate can result in an increase in fracture toughness. This occurs because the deformation heat does not have sufficient time to dissipate, creating an adiabatic condition where the localized temperature rise enhances the fracture toughness. This phenomenon is consistent with the dense layer of dimples observed on the fracture surface of the impact specimens and explains the difference in fracture type between the impact and tensile specimens of the weld.

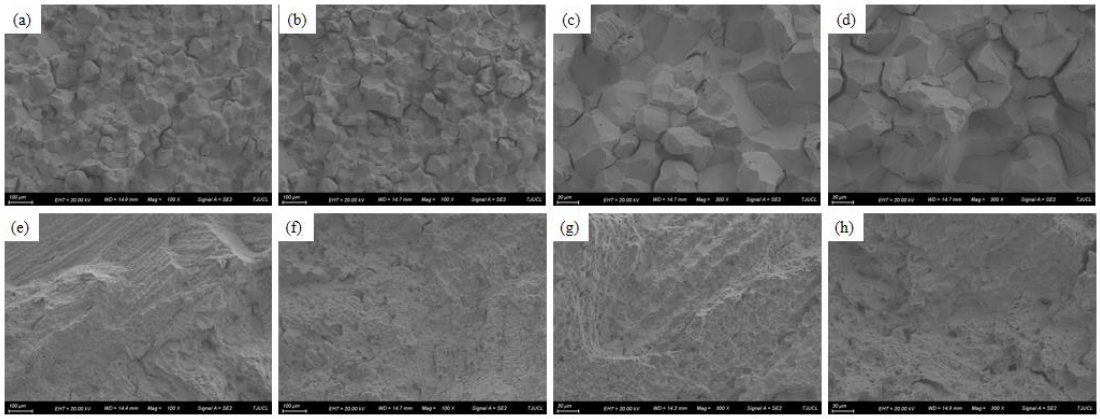

Figure 6. Typical fracture morphology of welded joint specimens after service: (a)–(d) Tensile fracture morphology and (e)–(h) impact fracture morphology

3.2. Analysis of Microstructure Results

3.2.1. Microstructure of HR3C Steel

Fig.7 shows the optical microstructure of HR3C steel after service. Before service, the metallographic structure of the steel consisted of equiaxed austenitic grains with straight subgrain boundaries [16-17]. After 4000 hours of service at 620°C, the grain boundaries became more distinct. A certain amount of point-like undissolved phase was observed in this region, and the grain-boundary precipitation phase was distributed in chains. The austenite and grain-boundary precipitates were mainly $M_{23}C_6$, while the intracrystalline point-like precipitates may be randomly distributed σ-phases. The σ-phase increases embrittlement, causes steel sensitization, reduces strength and plasticity, and adversely affects the mechanical properties of the joint.

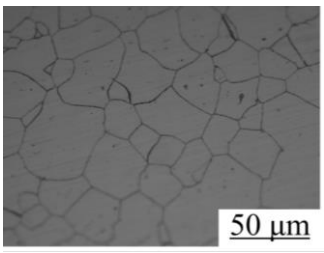

Figure 7. Metallographic organization of HR3C steel after service

Fig.8 shows the SEM image of HR3C steel after service. At the grain boundaries, continuous precipitates formed a chain-like structure; according to the EDS analysis, these precipitates are Cr enriched. Inside the grains and near the grain boundaries, dispersed, small granular precipitates and Nb-rich precipitates aggregated in lumps. Irregularly shaped voids appeared continuously along the grain boundaries of the precipitated phase and matrix. These voids grew, aggregated, and subsequently merged to form microcracks, negatively impacting the material's mechanical properties.

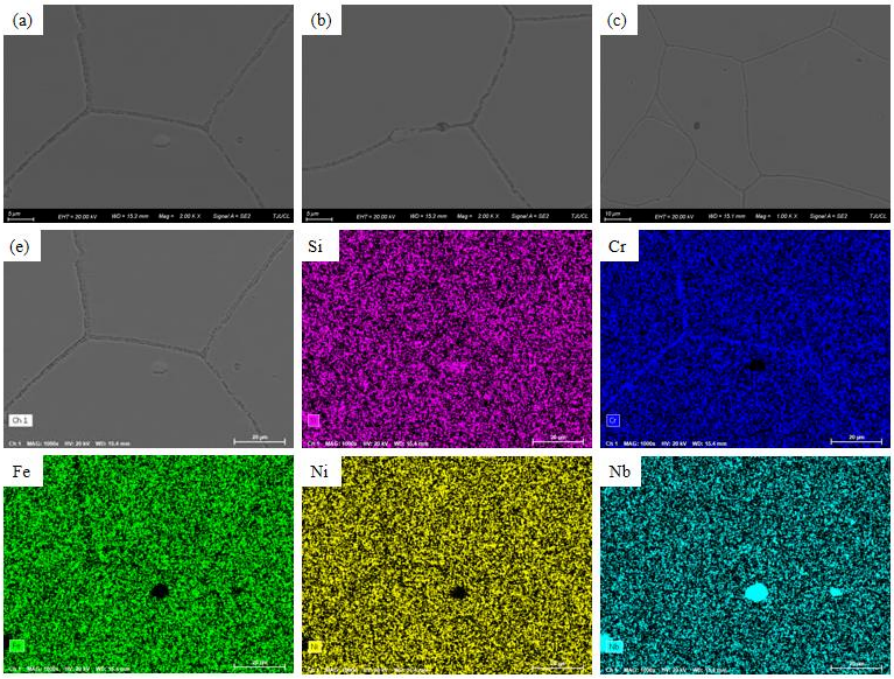

Figure 8. EDS element distribution of HR3C steel after service

Fig.9 shows the TEM microstructure of HR3C steel after service. The steel was significantly Cr enriched, while the Fe and Ni contents were lower at the grain boundaries. In the point-like precipitates, Nb was heavily enriched, while the Fe and Ni contents decreased. The Si distribution did not significantly change. The main chemical formula of the σ-phase is $(Fe, Ni)_x(Cr, Mo)_y$, which is enriched in Ni and Cr. However, this is inconsistent with the results of the elemental scans. Thus, the σ-phase was excluded, and the point-like precipitates were determined to be Nb-rich compounds. Compared with other precipitates, the σ-phase is more detrimental, and its precipitation must be prevented or strictly controlled.

Precipitates were generated at the grain boundaries and within the grains of HR3C tubes after service. The shadows in Fig.9(a) represent black needle-like precipitates within the grains. Fig.9(b)–(d) indicates continuous bead-like precipitation phases along the grain boundaries, and Fig.9(e),(f) shows large spherical and blocky precipitation phases within the grains. Through selected area electron diffraction calibration and energy spectrum analysis, the bead-like precipitation phase along the grain boundaries was identified to be mainly $M_{23}C_6$; the large spherical and blocky precipitation phases within the grains were $M_{23}C_6$ and a small amount of Nb(C,N); the long needle-like or rod-like precipitation phase near the grain boundary was the Cr-rich σ-phase; and the diffusely distributed, fine spherical or short, rod-like precipitation phase was the Z-phase, composed of NbCrN. HR3C steel had a stable austenitic structure before and after service. It is inferred that the changes in mechanical properties before and after service are mainly related to the size, morphology, and distribution of the precipitated phases. The size of the Z-phase in the HR3C steel base material and welds was mostly around tens of nanometers, diffusely distributed with high stability. The Z-phase precipitated not only within the crystal but also at the austenite grain boundaries and twin grain boundaries. The stable presence of finely dispersed Z-phases can impede dislocation motion, enhancing the strength and hardness of HR3C steel after aging. In addition, the intracrystalline, diffusely distributed $M_{23}C_6$ strengthens the HR3C steel to some extent, but its effect is weaker than that of the Z-phase owing to its larger size. The deterioration of the weld's impact toughness is mainly due to the precipitation of needle-like or short, rod-like σ-phases near the grain boundaries and the network distribution of the $M_{23}C_6$ phase, which can easily cause subsequent intergranular brittle fracture [18].

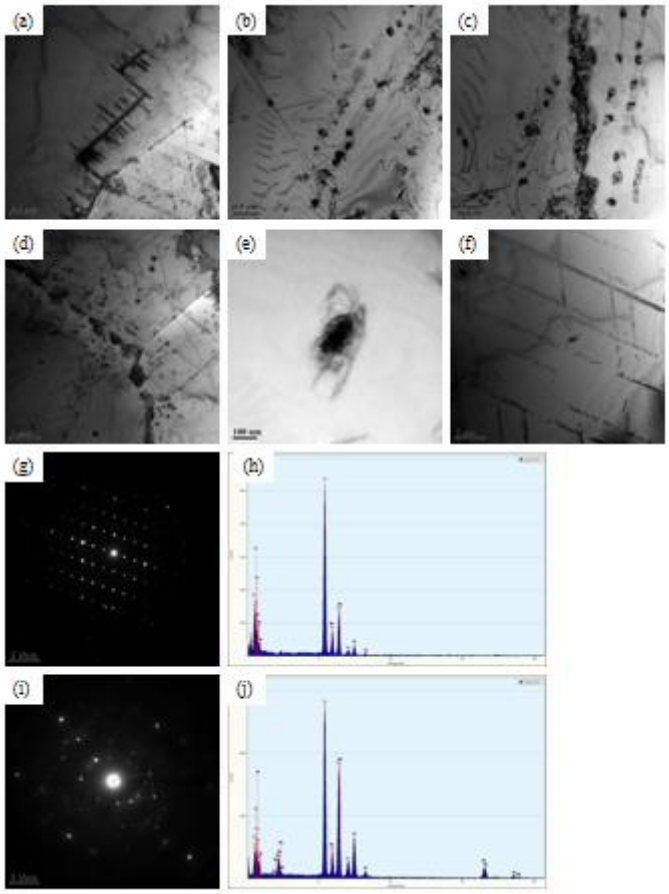

Figure 9. TEM microstructure of HR3C steel after service

3.2.2. Microstructure of Welded Joints

Fig.10 shows the OM of the welded joints after 4000 hours of service at 620°C. The microstructure of the welded joints was typically non-uniformly distributed austenite mainly composed of dendrites. The dendritic and cellular structures nucleated on the grains of the base material fusion zone and grew in the opposite direction of heat dissipation. After service, the dendritic structure in the weld coarsened. The number of carbides in the microstructure did not significantly change. In addition, black carbides were diffusely distributed within the dendritic structure.

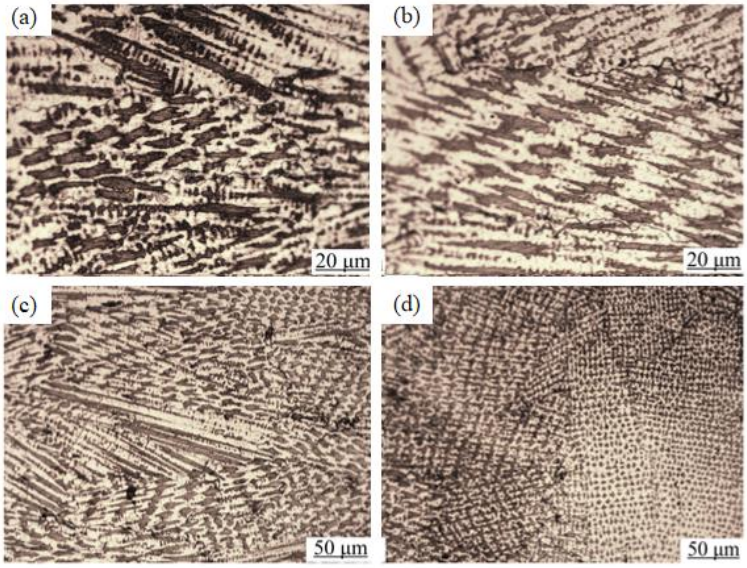

Figure 10. Optical microscopy images of metallographic structure of welded joints after service

Fig.11 shows the SEM image of the welded joints after service. From the Fig., it can be observed that the precipitates distributed at the grain boundaries and within the austenite grains were small. Some gray precipitates appeared on the grain boundaries, and the dark, intragranular point-like precipitates were large. The elemental distribution map of the welds after service was used to determine the concentration of each element in different regions based on the number and brightness of points representing each element. After service, Cr in the microstructure gradually diffused to the grain boundaries and the boundaries of the precipitation phase, while the Cr content inside the grains was relatively low. The Fe, Co, and Ni contents of the grain boundaries and point-like precipitates were reduced. In the point-like precipitates, Nb was significantly enriched, and Fe, Co, and Ni were sparse. Furthermore, the distribution of Si and Mn did not significantly change.

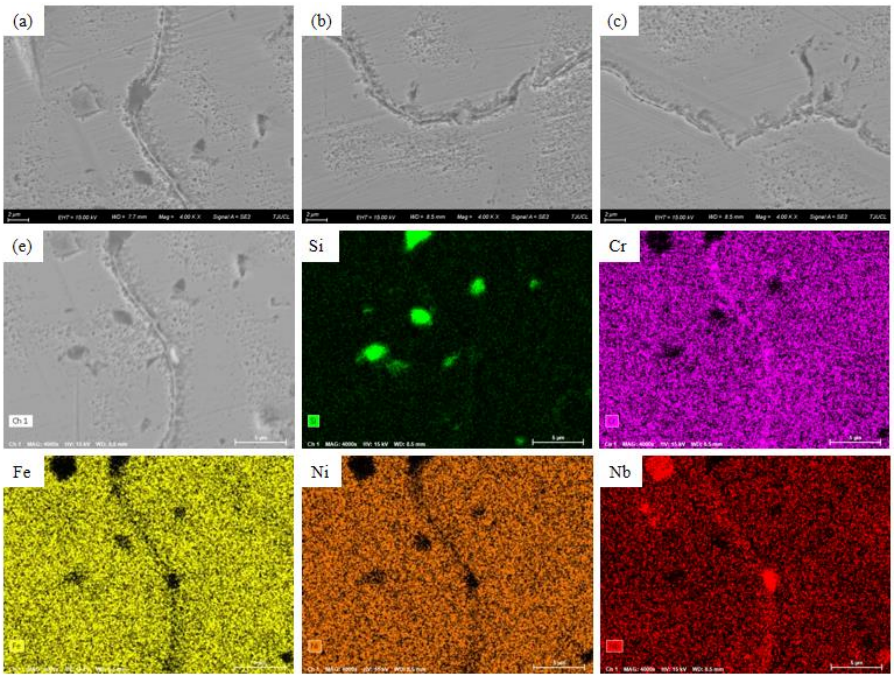

Figure 11. SEM microstructure and EDS elemental distribution of welded joints after service

Fig.12 shows the TEM microstructure of the welded joints after service. Precipitates were generated at the grain boundaries and within the crystals of the welded joints. Large spherical and long, lobe-shaped precipitation phases were observed within the crystals in Fig.12(a) and (i). The precipitated needle-like, elongated precipitates are shown in Fig.12(b)–(h), and the bead-like phase that precipitated continuously along the grain boundaries is shown in Fig.12(j). This bead-like phase mainly consisted of $M_{23}C_6$, while the large spherical and blocky intracrystalline precipitation phases constituted $M_{23}C_6$ and a small amount of Nb (C, N). As analyzed by selected area electron diffraction calibration and energy-dispersive X-ray spectroscopy, the long needle-like or rod-like precipitates near the grain boundaries were Cr-rich σ-phases. In addition, a small amount of blocky Si-rich phase, composed of Cr_3Ni_2SiC, was found near the grain boundaries. The fine spherical or short rod-like precipitated phase diffusely distributed in the welds was the Z-phase, which was composed of NbCrN.

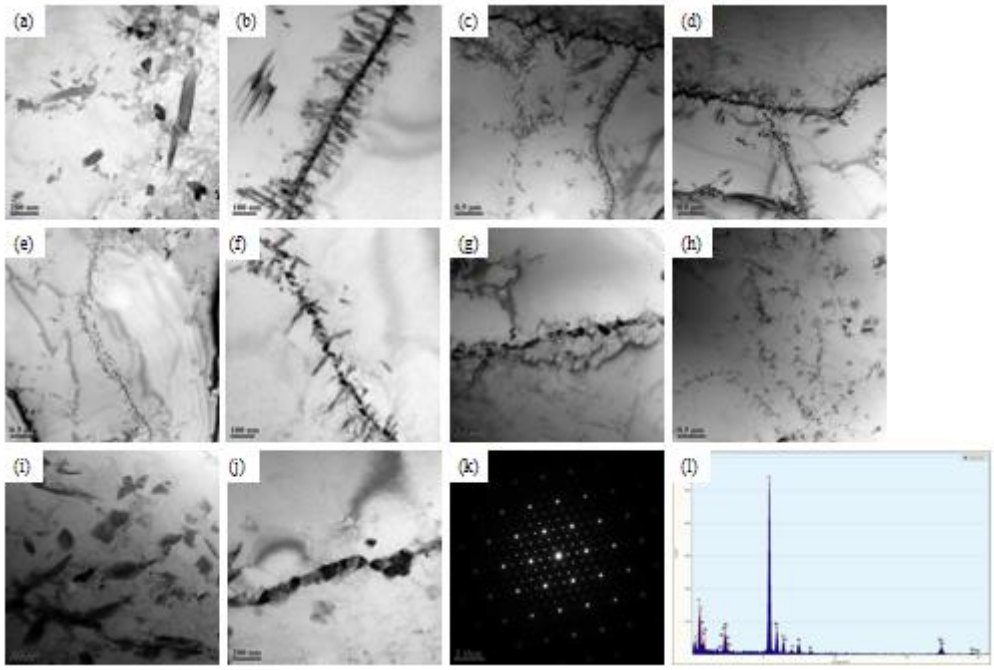

Figure 12. TEM microstructure of welded joints after service

3.3. Relationship between Changes in Microstructure and Mechanical Properties

Based on the above microstructural observations and mechanical property comparisons, the HR3C steel and welded joints have a stable austenitic microstructure before and after service. The size, morphology, and distribution of precipitated phases significantly affect the material's mechanical properties [19].

Before service, the HR3C steel contained a small amount of diffusely distributed, point-like precipitates at the grain boundaries and within the grains. After 4000 hours of service at 620 ℃, only a few point-like precipitates were observed within the grains of the base material. Continuous bead-like, long needle-like, or rod-shaped precipitates were distributed along the grain boundaries. The spherical or blocky precipitates within the grains were primarily Ni-rich NbCrN, while the continuous bead-like, long needle-like, or rod-shaped precipitates along the grain boundaries were mainly $M_{23}C_6$ phases [20].

After service, the NbCrN phase was detected in the HR3C steel and welded joints. NbCrN, a typical precipitate in austenitic stainless steels, has a significant hardening effect on the properties of these steels. Fine NbCrN particles can pin dislocations and thus enhance hardness [21]. During the microstructural evolution process, the grain size tends to increase and the number of twins tends to decrease, which subsequently affects the material's mechanical properties [22]. The impact properties, yield strength, and tensile strength of the HR3C steel and welded joints were poorer after service than before service. This degradation in mechanical properties is mainly attributed to the precipitation of needle-like, short-rod, and mesh-distributed $M_{23}C_6$ phases near the grain boundaries after service [23-25]. $M_{23}C_6$ carbide, as a metastable phase, is first formed in austenitic stainless steels and was observed during the early stages of precipitation. $M_{23}C_6$ carbides precipitated within the grains also grow at the grain boundaries and significantly widen them, imparting a pronounced coarsening effect [26]. The resulting Cr deficiency at the grain boundaries causes intergranular corrosion, making it more likely for defects such as voids to form; therefore, the coarsened carbides at the grain boundaries negatively impact grain-boundary strength [27]. This creates a pronounced tendency towards intergranular brittleness and facilitates the formation of brittle fractures along the grain boundaries [28-31]. As a result, the impact properties, yield strength, and tensile strength of the welded joints and base material (HR3C steel) are degraded after service.

4. Conclusions

The microstructural and mechanical properties of the welded joints of ultra-supercritical pipelines and the base material (HR3C steel) were investigated after 4000 hours of operation at 620 ℃. The following conclusions were drawn:

(1) Long-term service leads to the precipitation of more secondary phase particles in the welded joints and base material (HR3C steel). Among them, chain-like $M_{23}C_6$ carbides are concentrated along the grain boundaries, while granular NbCrN is mainly dispersed within the grains.

(2) The high-temperature creep environment causes the coarsening of $M_{23}C_6$ carbides at the grain boundaries, which is the main factor leading to the reduction in mechanical properties of the welded joints and base material (HR3C steel).

(3) After 4000 hours of creep at high temperatures, the finely dispersed NbCrN particles within the grains and their interaction with dislocations positively affect the mechanical properties of the welded joints and base material (HR3C steel). However, the gradual deposition of large NbCrN particles eventually degrades the mechanical properties.

References

[1] Yan, J. and Y. Gu, et al. "Evolution of microstructure and mechanical properties of a 25Cr-20Ni heat resistant alloy after long-term service." Materials Science and Engineering A 2016, 675, 289-298.

[2] He, J. and R. Sandström, et al. "Creep, low cycle fatigue and creep-fatigue properties of a modified HR3C." Procedia Structural Integrity 2016, 2, 871-878.

[3] Zhang, Y. and Q. Chang, et al. "Assessment of the creep damage in HR3C steel using the misorientation parameters derived from EBSD technique." Materials Letters 2022, 306, 130893.

[4] Zhang, Z. and Z. Hu, et al. "Microstructure evolution in HR3C austenitic steel during long-term creep at 650°C." Materials Science and Engineering A 2017, 681, 74-84.

[5] Hu, Z. and Z. Zhang. "Investigation the effect of precipitating characteristics on the creep behavior of HR3C austenitic steel at 650 ℃." Materials Science and Engineering A 2019, 742, 451-463.

[6] Li, Y. H. and S. Z. Wang, et al. "Corrosion of an Austenitic Heat-Resistant Steel HR3C in High-Temperature Steam and Supercritical Water." Materials Science 2014, 908, 67-71.

[7] Luo, K. and Y. Zhao, et al. "Embrittlement mechanism of austenitic heat resistant steel HR3C for ultra supercritical boiler." Transactions of Materials and Heat Treatment 2017, 38(7), 79-86.

[8] Zhou, J. and G. Xiang, et al. "Precipitates change and effect on hardness of HR3C steel after long-term service." Heat Treatment of Metals 2023, 48(9), 203-207.

[9] Zhang, Y. and H. Jing, et al. "Microstructure and texture study on an advanced heat-resistant alloy during creep." Materials Characterization 2017, 130, 156-172.

[10] Zhou, R. and L. Zhu. "Growth behavior and strengthening mechanism of Cu-rich particles in sanicro 25 austenitic heat-resistant steel after aging at 973 K." Materials Science and Engineering: A 2020, 796, 139973.

[11] Zieliński, A. and G. Golański, et al. "Evolution of the microstructure and mechanical properties of HR3C austenitic stainless steel after ageing for up to 30,000h at 650–750°C." Materials Science and Engineering: A 2020, 796, 139944.

[12] Gao, Z. and Z. Hu, et al. "Effect of on-site service for 16,000 and 38,000 h on microstructure and mechanical properties of austenitic steel HR3C reheater tubes." Engineering Failure Analysis 2023, 149, 107247.

[13] Zhou, Y. and Y. Liu, et al. "Precipitation and hot deformation behavior of austenitic heat-resistant steels: A review." Journal of Materials Science & Technology 2017, 33(12), 1448-1456.

[14] Yong, X. and X. Liu, et al. "First-Principles Calculate the Stability, Mechanical Properties and Electronic Structure of Carbide MC, M2C and M6C in M50NiL Steel." Materials. 2024, 17.

[15] Song, K. and L. Zhao, et al. "Dislocation creep modelling of Sanicro 25 based on microstructural evolution and particle hardening mechanism." Theoretical and Applied Fracture Mechanics 2021, 112, 102893.

[16] Zhang, J. and Z. Hu, et al. "Creep damage characteristics and evolution of HR3C austenitic steel during long term creep." Materials Science and Engineering: A 2022, 832, 142432.

[17] Zhang, Z. and Z. Gao, et al. "Three-dimensional characteristic and evolution of creep cavity and microcrack of HR3C austenitic heat resistant steel after long-term creep at 650 ℃." Engineering Failure Analysis 2024, 164, 108634.

[18] Zhang, Y. and H. Jing, et al. "High-temperature deformation and fracture mechanisms of an advanced heat resistant Fe-Cr-Ni alloy." Materials Science and Engineering: A 2017, 686, 102-112.

[19] Bai, J. M. and Y. Yuan, et al. "Effect of carbon on microstructure and mechanical properties of HR3C type heat resistant steels." Materials Science and Engineering: A 2020, 784, 138943.

[20] Wang, X. and L. Xu, et al. "Inhibition of the intergranular brittleness of HR3C heat-resistant steel by strain-aging induced nano-M23C6 dispersion precipitation." Journal of Materials Science & Technology 2024.

[21] WANG, B. and Z. LIU, et al. "Microstructure Evolution and Mechanical Properties of HR3C Steel during Long-term Aging at High Temperature." Journal of Iron and Steel Research, International 2014, 21(8), 765-773.

[22] Wang, Q. and R. Xin, et al. "Microstructure and its effect on high temperature tensile properties of T92/HR3C dissimilar weld joints." Journal of Manufacturing Processes 2022, 82, 792-799.

[23] Sklenička, V. and K. Kuchařová, et al. "Creep properties of simulated heat-affected zone of HR3C austenitic steel." Materials Characterization 2017, 128, 238-247.

[24] Yin, Z. and Y. Zhou, et al. "Effect on Steam Oxidation Behavior of HR3C Austenitic Steels at 700 ℃." Surface Technology 2020, 49(12), 267-273.

[25] Zhu, C. Z. and Y. Yuan, et al. "A Modified HR3C Austenitic Heat-Resistant Steel for Ultra-supercritical Power Plants Applications Beyond 650 A°C." Metallurgical and Materials Transactions A-Physical Metallurgy and Materials Science 2018, 49(2), 434-438.

[26] Yuan, J. and W. Wang, et al. "Investigation into the failure mechanism of chromia scale thermally grown on an austenitic stainless steel in pure steam." Corrosion Science 2016, 109, 36-42.

[27] Peng, B. and M. Zhang, et al. "DIC/DSI based studies on the local mechanical behaviors of HR3C/T92 dissimilar welded joint during plastic deformation." Materials Science and Engineering: A 2022, 857, 144073.

[28] Boulesteix, C. and F. Pedraza. "Characterisation of aluminium diffusion coatings elaborated on austenitic stainless steels and on ferritic-martensitic steels." Surface and Coatings Technology 2018, 339, 27-36.

[29] Gan, L. and B. Zhu, et al. "Micro-mechanics investigation of heterogeneous deformation fields and crack initiation driven by the local stored energy density in austenitic stainless steel welded joints." Journal of The Mechanics and Physics of Solids 2024, 188, 105652.

[30] Kang, J. and Q. Wang, et al. "Fatigue fracture mechanism of T92/HR3C dissimilar metal weld joints at elevated temperature." Materials Characterization 2022, 190, 112081.

[31] Saca, N. and L. Radu, et al. "Investigation of Physical-Mechanical Properties and Microstructure of Mortars with Perlite and Thermal-Treated Materials." Materials 2024, 17.